C. R. Mecanique 338 (2010) 688–697

Contents lists available at ScienceDirect

Comptes Rendus Mecanique

www.sciencedirect.com

Physical analysis of velocity and temperature cross-correlations in a plane mixing layer using variable temperature hot wire anemometry

Malick Ndoye [a,b,c,*], E. Dorignac [b], J. Delville [b], G. Arroyo [a,c]

[a] Cemagref, UR TERE, 17 Avenue de Cucillé, CS64427, F-35044 Rennes, France
[b] Institut PPRIME, CNRS – Université de Poitiers – ENSMA UPR 3346, F-86036 Poitiers, France
[c] Université Européenne de Bretagne, Rennes, France

ARTICLE INFO

Article history:
Received 13 July 2010
Accepted after revision 8 October 2010
Available online 4 November 2010

Keywords:
Turbulence
Mixing
Heat flux
Hot wire anemometry
Multiple overheat
Quadrant decomposition
Plane mixing layer

ABSTRACT

Velocity–temperature cross-correlations were investigated in a non-isothermal mixing layer generated by two air flows at different velocities and temperatures. The study focused on the analysis of heat transfer across turbulent free shear flows in air like air curtains or wide wall jets. A new hot wire anemometry technique was used to obtain simultaneous measurements of velocity and temperature at the same location with a single wire. The hot wire was operated following the multiple overheat principle, consisting in reproducing a given sequence comprising several successive steps in the overheat applied to the wire at a frequency of 1000 to 10,000 Hz. The synchronism of the velocity and temperature measurements allowed a fine analysis of the relationship between the fluctuations of the two physical quantities considered. These relationships were first analyzed using a conditional probability density function approach that allowed the description of the evolution of the temperature fluctuation T' across the mixing layer associated with both a fully turbulent mixing process and intermittencies. Finally, by splitting the heat flux $u'(t) \times T'(t)$ into four quadrants, classically defined as the contributions of the four possible combinations of the instantaneous values of the fluctuations $u'(t)$ and $T'(t)$ according to their respective signs, the intermittent part of the heat flux associated with the saddle point ejections was shown to be progressively more dominant in the mixing process evolving along the self-similarity region of the flow.

1. Introduction

Transport of a scalar, such as temperature or a concentration, by a mixing layer type flow is a key issue for many industrial applications and environmental flows. We particularly consider the local control of thermal environments, which is an important concern in industry. Studies are being performed in our laboratories to improve thermal confinement by mixing reduction in situations of mixing layer type. In this category of shear flows, the temperature mixing process is closely linked to the mechanical stirring imposed by the velocity field. It is therefore necessary to understand the inherent coupling between velocity and temperature fields. This coupling is present in the scalar transport equations in terms of a vectorial heat flux, one component of which is $\overline{u'T'}$.

Most of the past studies on scalar mixing layers (temperature, concentration and/or density) emphasized the differences between dynamic and scalar behaviors. Faster and greater development is generally observed in the dynamic field compared to the scalar field. In his study of a heated plane mixing layer with a zero velocity ratio, Fiedler [1] observed dissymmetrical

* Corresponding author.
E-mail address: malick.ndoye@lea.univ-poiters.fr (M. Ndoye).

1631-0721/$ – see front matter
doi:10.1016/j.crme.2010.10.006

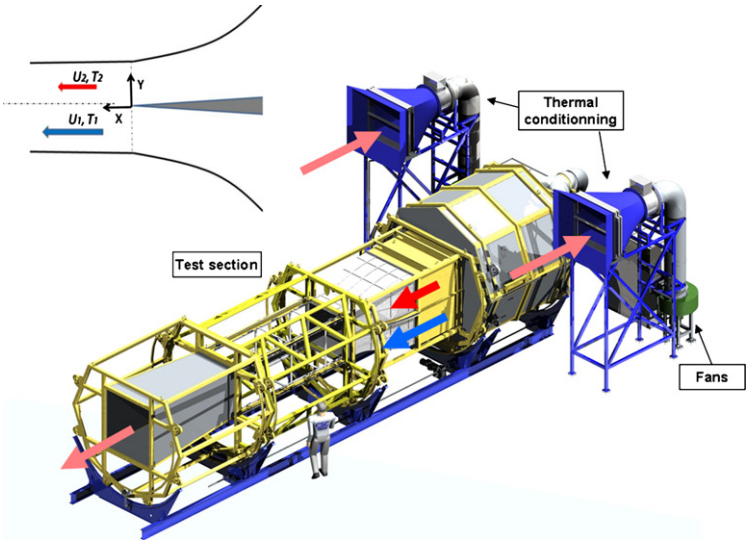

Fig. 1. Diagrammatic representation of the low-speed wind tunnel (right) and flow configuration (left).

average and RMS temperature profiles, with a triple inflexion point and a bi-modal shape, respectively, compared to those of the velocity field. Similar results were also obtained in gaseous mixing layer studies by Brown and Roshko [2], Batt [3] and Masutani and Bowman [4], and, more recently, in simulations of heat transfer by Bisset [5]. Probability density functions (PDF) are commonly used to describe the scalar mixing process. Two categories of scalar PDF can generally be obtained in the mixing layer, the marching type or the non-marching type, as denoted among others by Bisset [5] and Pickett and Ghandi [6,7] in their Planar Laser Induced Velocimetry scalar measurement in an incompressible mixing layer. Marching means here that the shape of the PDF continuously evolves as the measurement point is moved across the mixing layer. Karasso and Mungal [8] stated that the final stage of a high Reynolds mixing layer is characterized by marching type PDFs of the scalar.

The aim of the present study, based on heat flux measurements in a non-isothermal low-speed plane mixing layer, was to analyze the mechanism of the velocity–temperature interactions responsible for scalar transport. Analysis of velocity–temperature coupling requires the understanding of instantaneous joint distributions of these two quantities. We chose therefore to use a novel multiple overheat hot wire anemometer developed in our laboratories. This technique provides simultaneous measurement of velocity and temperature fluctuations at the same point with a single wire, thus allowing fine analysis of turbulence based on correlations, conditional density probabilities and quadrant decomposition of the heat flux [9].

After a short presentation of the experimental apparatus, we provide a detailed description of the measurement method used. The results of the flow characterization are then set out. From a conditional PDF analysis of the velocity and temperature fluctuations and quadrant decomposition of the heat flux, we discuss the results on cross-correlations.

2. Wind tunnel

The experiments were conducted in a specific open-loop wind tunnel equipped with two independent aeraulic circuits, as shown in Fig. 1. Each is equipped with a 7.5 kW blower, a 42 kW cold battery and a 31 kW heater. Two parallel air streams are blown separately through two independent halves of a conditioning chamber comprising several screens and a slowly converging part (contration ratio: 2.25). The two streams are separated by a 52 mm thick thermal insulating plate. They then merge and initiate the mixing process downstream of the sharp end of a 1.5° tapered splitter plate made of aluminium. The mixing layer expands in a test section which is 3 m long and 1 m $\times$ 1 m in cross section. Downstream from the test section, the mixed flux is evacuated through a diverger.

The velocity and the temperature of the two parallel streams were set up separately in a range of 0.5 to 5 m/s and 5 to 35 °C. The experiments were carried out in stabilized conditions, providing velocity ratios ranging from $r = 0.33$ to $r = 0.77$ and temperature differences ranging from 0 to 25 K. The stable configuration studied, with the hot layer above the cold one, corresponds to the industrial and atmospheric situations that motivated the study (stable separation of a lower cold layer from a warm atmosphere).

At the entrance of the test section, the turbulence levels in the two parallel streams before mixing were lower than 1% for velocity and around 0.05 °C for temperature. Classically, the growth of the mixing layer from its physical origin (trailing edge of the separating plate) depends on the state of the boundary layers developed upstream on both sides of the plate. A tripping device (a narrow blade forming a 8 mm high saw tooth shaped obstacle) was placed on both sides of the thick plate upstream from the contraction cone in order to obtain similar turbulent boundary layer conditions for all the flow

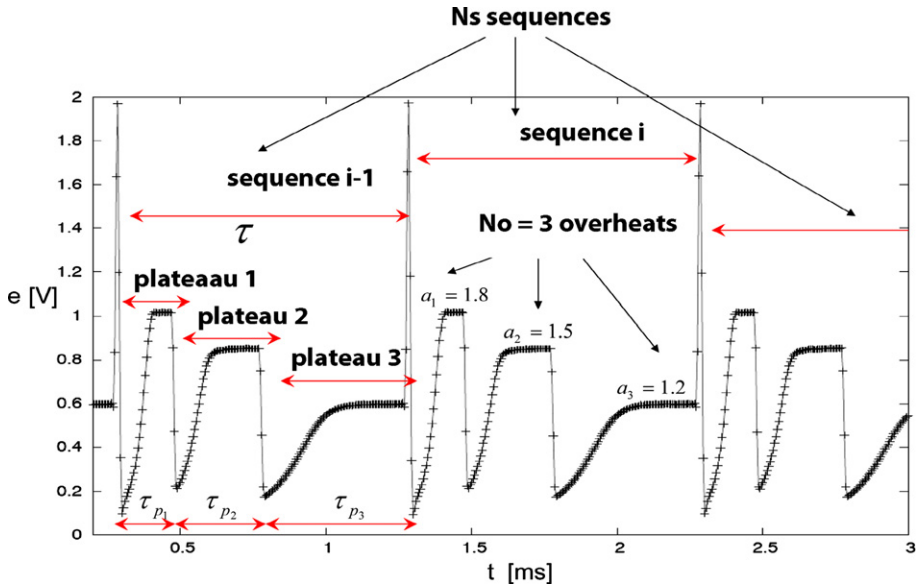

Fig. 2. Typical time trace of PCTA output voltage, with multiple overheat sequences of three overheat levels.

configurations tested. The thicknesses of the dynamic boundary layers measured at the entrance to the test section were $\Theta_{H.S.} = 2.37$ mm on the high speed side and $\Theta_{L.S.} = 2.45$ mm on the low speed side of the trailing edge of the splitter plate. The thickness of the thermal boundary layer was around 10 mm which is rather large due to the upstream thermal transfer through the sharp end of the splitter plate, but reasonably small for such experimental conditions.

3. Measurement system

Measurements were performed using a W-Pt hot wire probe (2.5 µm diameter, 0.5 mm long) connected to a new variable temperature hot wire anemometer operating sequentially at three consecutive overheat ratios. This anemometer was specially designed and implemented for the simultaneous measurement of velocity and temperature at the same point with a single wire. The principle developed, named PCTA (Parameterisable Constant Temperature Anemometer), is based on the multiple overheat principle and on specific signal processing. More details on the principle and methods implemented on the PCTA can be found in [9].

3.1. Multiple overheat principle

The PCTA anemometer uses the classical Constant Temperature Anemometer technique described by Bruun [10] and Perry [11]. Knowing that the wire is principally sensitive to velocity for high overheat levels (hot wire) and principally sensitive to temperature for low overheat levels (cold wire), various authors have used a multiple overheat principle for the simultaneous measurement of flow velocity and temperature, with either parallel wires or a sequence of different overheats applied to a single wire (Corrsin [12] and Verollet [13] for subsonic flows, Kovasznay [14], Walker [15] and Weiss et al. [16] for supersonic flows, and Saez [17] for mixed convection measurement). Due to the limitations in the physical principle and in the signal processing procedure, the authors achieved access to velocity and temperature moments up to the third order, but not to instantaneous velocity and temperature distributions at high frequencies.

3.2. PCTA principle

The PCTA principle is based on the implementation of a specific design allowing both rapid overheating and periodic variation in the overheat of the wire, making hence possible the reproduction of a unitary sequence of successive overheat levels at a constant frequency. The typical evolution of a triple overheat sequence is shown in Fig. 2. The number of overheat levels per sequence can vary from 2 to 8. The overheat duration can be set between 100 and 1000 µs to provide access to simultaneous high frequency velocity and temperature measurements at the same point. A minimization procedure allows the identification of instantaneous U and T decorrelated values from the data acquisition. The acquisition frequency can reach several kHz with a sufficiently thin wire. The performance of the PCTA is closely linked to the use of a dynamic calibration method in which the probe measures a periodically varying velocity associated with a decreasing temperature in a specific calibration wind tunnel. The principles of calibration, measurement and post-processing can be found in [9,18]. Only the main features of the method are recalled here.

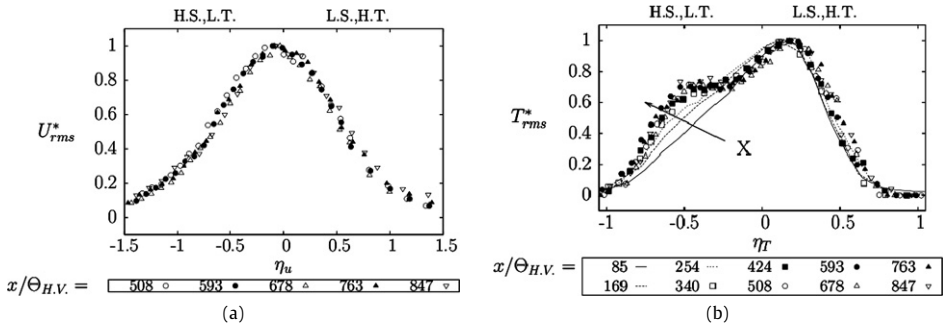

Fig. 3. Transverse profiles of (a) velocity and (b) temperature RMS fluctuations measured at different streamwise positions for $r = 0.50$, $\Delta T = 25$ K. RMS values of velocity U^*_{rms} and temperature T^*_{rms} are normalized according to their local maximum value.

3.3. Calibration and signal processing

The equation describing the relationship between a hot wire voltage response and the velocity–temperature couple (U, T) in a non-isothermal fluid flow can be chosen from various non-linear heat transfer equations, as described in particular by Bruun [10]. In the present study we used an extended King's law:

$$e^2 = \left(a + bU^n\right)(T_w - T) \tag{1}$$

where e is the instantaneous voltage measured, and U and T are unknown. The wire temperature T_w, the coefficients a, b, and the exponent n are parameters associated with a given overheat level. For each overheat level of subscript k, within the overheat sequence of subscript i, the voltage measured is expressed as:

$$e^2_{i,k} = \left(a_k + b_k U_i^{n_k}\right)(T_{w,k} - T_i) \tag{2}$$

A single voltage value is automatically extracted for each overheat level assuming two important hypotheses: (i) the repeatability of the overheat application is such that the parameters a, b, n and T_w are valid for a given overheat level on the whole set of sequences acquired, (ii) U and T are considered constant on a given overheat sequence, which is equivalent to low pass filter U and T variations at the repetition frequency of the sequences. An optimization procedure, based on the Levenberg–Marquardt algorithms,[1] is applied to extract the vectors of parameter $\mathbf{A}_k = \mathbf{a}_k, \mathbf{b}_k, \mathbf{n}_k, \mathbf{T}_{w,k}$ for each overheat level k, using calibration data. Another Levenberg–Marquardt procedure is applied to the instantaneous voltages in order to extract the velocity and temperature pairs (U_i, T_i) for each sequence integrated over the duration of the ith multiple overheat sequence. The accuracy of the PCTA method was evaluated by estimating successively the uncertainty associated with the dynamic calibration, the measurement procedure and the post-processing technique, using a Monte Carlo simulation method according to the recommendations in [20]. The results of this uncertainty estimation can be found in [9]. For the PCTA operating in a three overheats configuration as shown in Fig. 2, and a calibration sample size of 3×10^5, the uncertainties are 1% for velocity and 0.15 K for temperature.

4. Flow characterization

The PCTA principle was applied with a single wire placed parallel to the spanwise direction of the mixing layer in order to measure the streamwise U component of the velocity and its fluctuations u' defined by:

$$U(t) = u'(t) + \langle u \rangle \tag{3}$$

The development of the thermal field was found to follow a specific behavior in terms of transverse profile shape, thickness, expansion and dissymmetry across the longitudinal axis, compared to that of the velocity field. The mean temperature profiles exhibited a particular shape, characterized by a noticeable triple inflexion point compared to the mean velocity profiles. This classical passive scalar behavior was in line with previous scalar mixing studies by Masutani and Bowman [4], Fiedler [1], Brown and Roshko [2] and Koochesfahani and Dimotakis [21]. This dissymmetrical trend was repeated in the RMS temperature profiles, which presented double-peaked structure unlike the velocity RMS profiles, as depicted in Fig. 3. In the following figures showing transverse profiles across the mixing layer, the transverse coordinate y is replaced by the normalized coordinates, η_u for the velocity related curves and η_T for the temperature related curves. These normalized coordinates were defined in relation to the similarity references δ_ω and δ_T, which are the vorticity thickness and the thermal thickness of the mixing layer at the x location considered. The origins of these two normalized coordinates were positioned at the centre of the dynamic and thermal mixing layers, respectively, the physical coordinates of which were

[1] The general principle of the Levenberg–Marquardt algorithms can be found in *Numerical Recipes in Fortran* [19].

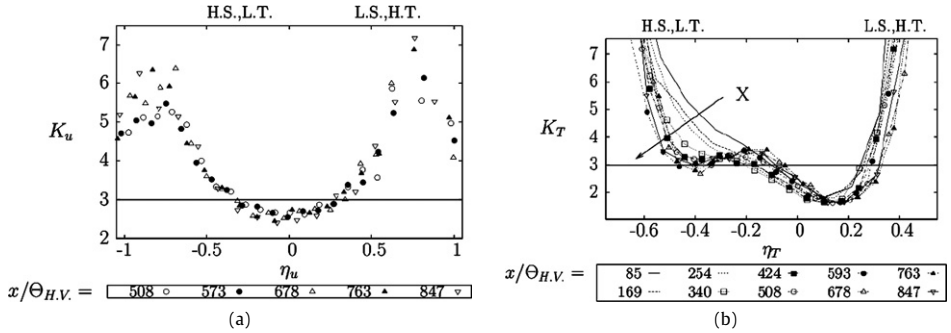

Fig. 4. Flatness factor: (a) velocity, (b) temperature; $r = 0.50$, $\Delta T = 25$ K. The horizontal line corresponds to the Gaussian value of 3.

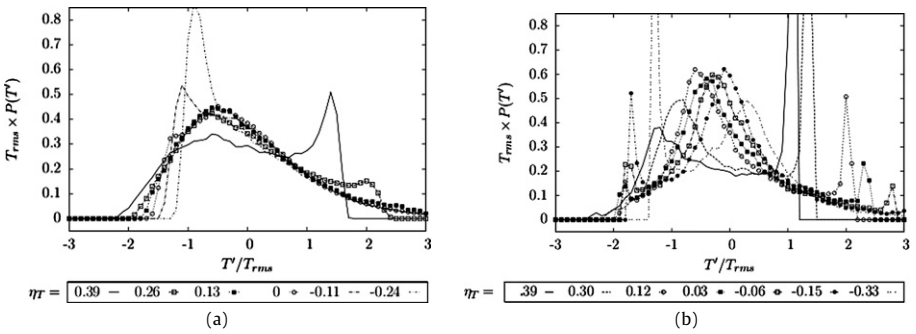

Fig. 5. Typical examples of non-marching (a) and marching (b) temperature PDF for different transverse positions across the layer at two given streamwise locations for $r = 0.50$, $\Delta T = 25$ K.

$y_{0.5u}$ and $y_{0.5T}$, these two values being different as a result of the differences in the deflections of the mixing layers from the symmetry plane of the test section. The definition of the normalized coordinates are:

$$\eta_u = (y - y_{0.5u})/\delta_\omega, \quad \text{and} \quad \eta_T = (y - y_{0.5T})/\delta_T \tag{4}$$

These figures and the related text refer systematically to a reference case corresponding to $r = 0.50$ and $\Delta T = 25$ K, being representative of the flow features that we could observe and analyze. The subscripts HS, LT and LS, HT relate to the conditions applied on both sides of the mixing layer, i.e. High/Low Speed and Temperature. Classically, the peak values of both velocity and temperature fluctuations tended to decrease with the downstream distance, as a result of the continuous increase in mixing as the fluid moved downstream, before stabilizing. The development distance of the flow (distance of appearance of the self-similarity of the fluctuations) appeared at about $x/\Theta_{H.S.} = 500$.

5. PDF analysis

The mixing process was investigated through the PDFs of temperature and velocity at various positions.

5.1. Flatness factor

The transverse evolution of the flatness factor (peak-related symmetry of the PDFs) of velocity and temperature fluctuations is depicted in Fig. 4 for various streamwise positions. The velocity flatness K_u presents similar distributions very close to the Gaussian value of 3 in the mixing region, highly peaked in the outer region and finally decreasing outside the mixing layer. The distributions of temperature flatness are strikingly different: initially skewed on one side towards a value of 2 in the development region, they switch progressively to a bimodal shape after the development distance. This final trend, also reported by Fiedler [1], is characterized here by values of K_T slightly greater than 3 near the mixing layer axis but decreasing towards markedly different minima down to 2 before increasing in the outer region. This streamwise evolution of K_T, related to the appearance of the temperature fluctuations in Fig. 3, suggests a noticeable variation in temperature PDF shape with the Reynolds number Re_x (related to the mixing layer width) and with the transverse position in the mixed region.

5.2. PDF shape

Velocity PDFs were found to be nearly gaussian in the central region of the mixing layer and strongly asymmetric in the outer region on both sides. Temperature PDFs are shown in Fig. 5 for various transverse positions across the shear layer

at two streamwise positions, selected to represent the changes occurring in the flow along x. At the end of the splitter plate wake region, where coherent structures appeared in the flow, the temperature PDF exhibited a single peak (most probable value of the temperature) markedly independent of the transverse position in the mixing layer. This particular behavior, named *non-marching* [8,21], is generally characteristic of mixing dominated by large-scale structures engulfing fluid originating from the uniform parts of the flow. After the fluctuating velocity and temperature fields have reached self-similarity, the PDFs switch to a *marching* behavior type [8,21] with a single peak the position of which varies across the layer by following the local mean value of the temperature. This particular trend is characteristic of mixing dominated by small flow scales.

A comprehensive examination of this non-gaussian behavior is provided hereafter through conditional analysis to provide insight into the double-peaked structure of the temperature fluctuations.

5.3. Conditional PDF analysis

The measured temperature probability density function, $p(T')$, verifies the equation:

$$\int_{-\infty}^{+\infty} p(T') = \int_{-\infty}^{+\infty} p(T')\big|_{u'<0} + \int_{-\infty}^{+\infty} p(T')\big|_{u'\geqslant 0} = 1 \tag{5}$$

where $p(T')|_{u'<0}$ and $p(T')|_{u'\geqslant 0}$ are conditional PDF temperatures associated with the occurrence of negative or positive velocity fluctuations, respectively. Figs. 6(a)–(g) show the conditional temperature PDFs obtained at different positions across the layer for a given streamwise location in the self-similarity region. This figure is composed by seven graphs from (a) to (g), each corresponding to a measurement point at a given transverse position η_u for the streamwise position $x/\Theta_{H.S.} = 593$. These were chosen in order to traverse the mixing layer depth at the given position x from the cold, rapid side to the hot, slow side. In each of these graphs, there are four curves representing the conditional PDFs, $p(T')|_{u'<0}$ and $p(T')|_{u'\geqslant 0}$, the total temperature PDF, $p(T')$, and the best Gaussian curve fitting the total PDF. The generally observed tendencies, whatever the position x in the developed region, are as follows.

- In the uniform flow region on both sides of the mixing zone (a and g), conditional PDFs and temperature PDF are very cramped, with a mode greater than 0.4 (maximum value of the corresponding Gaussian fit). Both peaks for PDFs conditioned by $u' < 0$ and $u' \geqslant 0$ are on the same side, showing fluctuations always associated with the corresponding hot or cold side. The temperature fluctuations are still dominated by the hot or cold limit corresponding to the temperature of the uniform part of the flow.
- In the proximity of the edges (b) and (f) of the mixing layer, PDFs strongly depart from gaussianity (showed here by a dashed line). This dissymmetry is related to the non-equivalent contributions of temperature fluctuations associated with $u' \geqslant 0$ and $u' < 0$. For example, at the edge of the hot, slow side ($\eta > 0$) the temperature PDF shows a peak corresponding to hot fluid associated with low speed, but with a significant integral contribution of entries of cold fluid ($T' < 0$) with higher speed ($u' > 0$) from the other side of the mixing layer. This high level of dissymmetry of the temperature PDF shows the coexistence of blobs of barely mixed hot, slow fluid (characterized by strongly dissymmetrical $p(T')|_{u'<0}$) and a more turbulent flow region, characterized by symmetrical $p(T')|_{u'\geqslant 0}$, very close to gaussianity, with fluctuations ranging from $-2 \times T_{rms}$ to $2 \times T_{rms}$. The inverse phenomenon arises at the other side. Thus the edges are very intermittent.
- The further we depart from the edges, in the direction of the mixing layer axis ((b) to (d) through (c), or (f) to (d) through (e)), the less the flow is influenced by the intermittencies arising from the edges. Therefore the peak characterizing the $p(T')|_{u'\geqslant 0}$ or $p(T')|_{u'<0}$ PDF decreases gradually. The fluid originating from both sides of the mixing layer is in a situation of turbulent mixing, more and more dominating as we move closer to the axis of the mixing layer where the total and conditional PDFs are very close to gaussianity.

6. Quadrant splitting analysis of the longitudinal heat flux

As suggested by the analysis of the conditional PDFs, the mixing can be seen as the sum of different processes in relation to the positivity or negativity of the product $u'(t) \times T'(t)$. In a second stage, the mixing process was analyzed with a quadrant splitting method as introduced by Lu and Willmarth [22]. This provides a comprehensive study of the contributions to the heat flux from the principal fluid motions within the flow. The method consists in splitting the instantaneous heat flux $u'(t) \times T'(t)$ into four quadrants, each being associated with one of the four possible combinations of the instantaneous values of the fluctuations $u'(t)$ and $T'(t)$ according to their positivity or negativity: *I*: $(u' > 0, T' > 0)$, *II*: $(u' < 0, T' > 0)$, *III*: $(u' < 0, T' < 0)$, and *IV*: $(u' > 0, T' < 0)$. A diagram of quadrant splitting is shown in Fig. 7. The time-average of $u'(t) \times T'(t)$ in each quadrant was calculated, providing four conditionally averaged values of the heat flux at each measurement point.

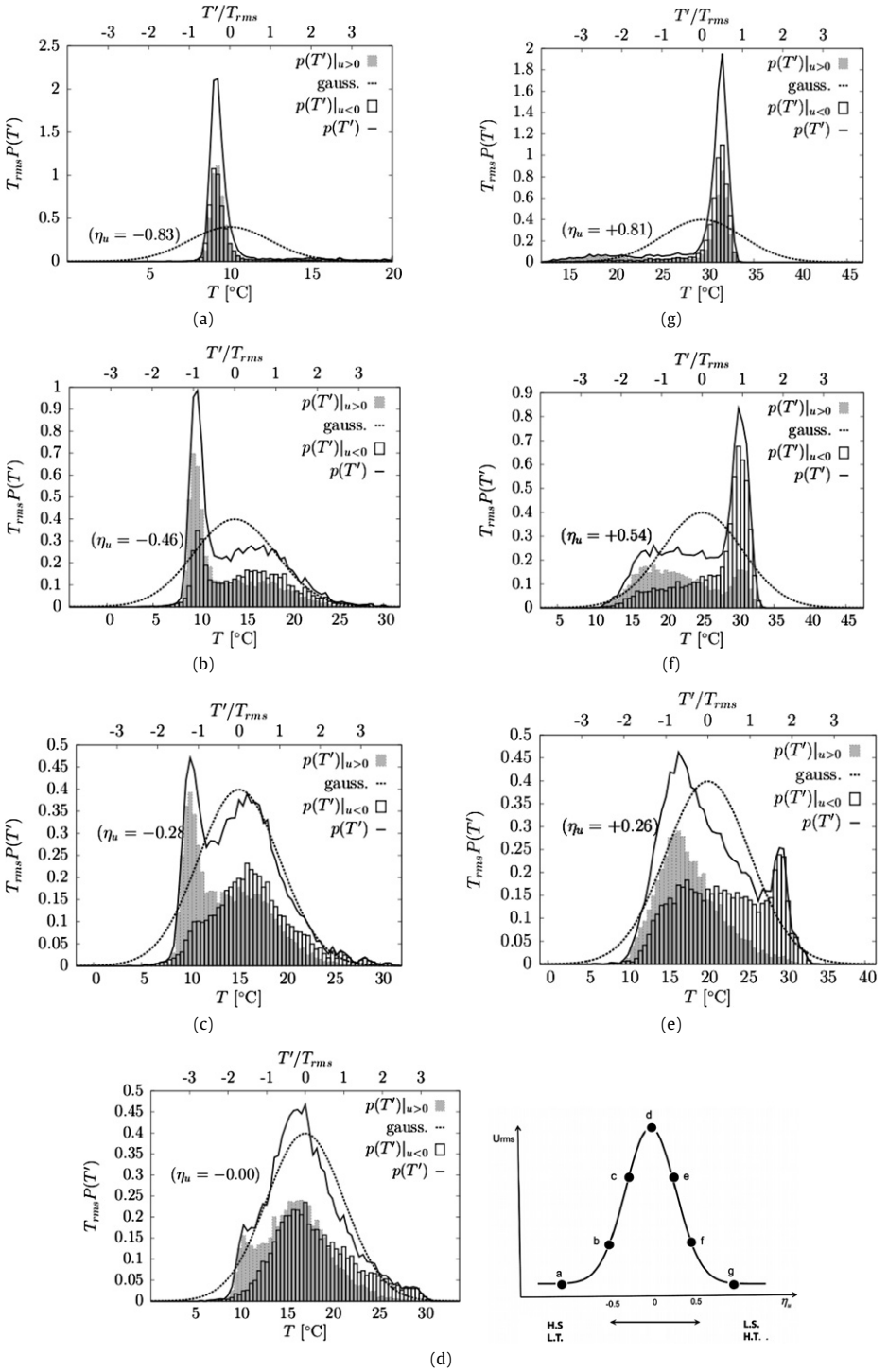

Fig. 6. (a)–(g) Variations in temperature PDF across the mixing layer conditioned by the negativity/positivity of the velocity fluctuations at the streamwise location $x/\Theta_{H.S.} = 593$ for $r = 0.50$, $\Delta T = 25$ K. The position of the corresponding measurement points are indicated in the bottom right graph.

6.1. Identification of the fluid movements corresponding to the quadrants

Fig. 8 illustrates the classical mixing layer flow topology, and makes it possible to distinguish two types of macroscopic structures: large eddies and strands (fine zones that surround these eddies). At the centre of the strand between two cores, lies a saddle point. Velocity and temperature fluctuation skewness presented in Fig. 9, shows that the predominant contribution to the fluctuation skewness (dominant intermittent events) are opposite for velocity fluctuations u' and temperature

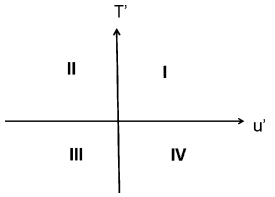

Fig. 7. Diagrammatic representation of the four quadrant.

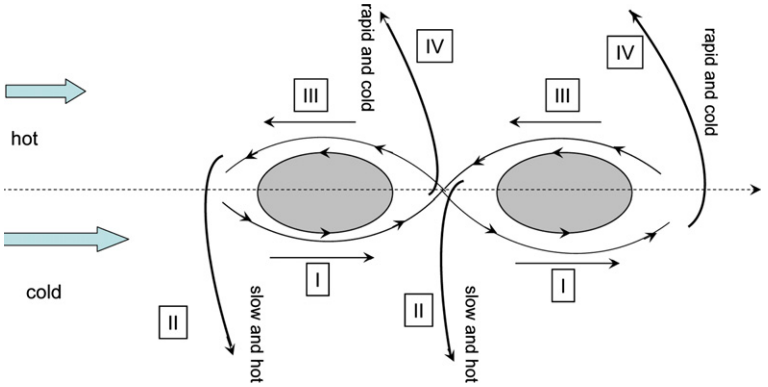

Fig. 8. Diagrammatic representation of principal fluid movements contributing to the heat flux in a non-isothermal mixing layer.

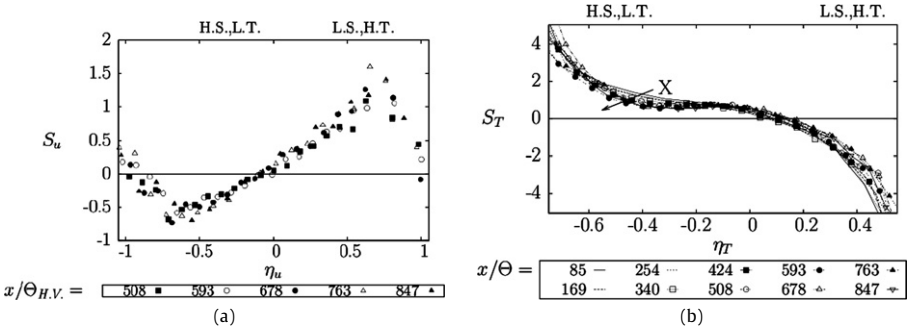

Fig. 9. Skewness factor: (a) velocity, (b) temperature; $r = 0.50$, $\Delta T = 25$ K.

fluctuations T'. Furthermore, saddle points are regions of significant fluid ejection out of the mixing layer. Each ejection produces an acceleration of the flow on the slow side and a deceleration on the rapid side, with vertical velocity fluctuations and longitudinal velocity fluctuations of opposing signs.

For example, in the present configuration, the rapid, cold uniform flow stream tends to strip off fluid intermittently from the saddle points. The mean temperature of this fluid originating from the cores is greater than the cold temperature, and its mean velocity is lower than the rapid velocity. Thus some hotter and slower fluids (leading to $T' > 0$ and $u' < 0$) are ejected from the saddle points towards the cold side, corresponding to quadrant *II*.

Similarly, the region of uniform hot, slow flow strips off some cold fluid from the saddle points. The fluid originating from such ejections is colder and faster than the uniform part of the flow on that side, corresponding to quadrant *IV*. From similar analysis it appears that quadrants *I* and *III* correspond to interactions between the periphery of the structures and the outer regions of uniform flow.

6.2. Analysis

The distributions of the four quadrants contributions are shown in Fig. 10 for different x positions, each corresponding to a graph. Each one graph shows the transverse profiles of $\overline{u'(t) \times T'(t)}$ separated into four curves, each corresponding to a quadrant. The magnitude of $\overline{u'(t) \times T'(t)}$ is representative of the relative strengths of the four contributions to the heat flux. In the initial wake region, the contributions of the different quadrants have comparable magnitudes. Downstream, the contributions of *I* and *III* evolve towards profiles shifted on opposite sides of an axis of symmetry located on the axis of the dynamic mixing region ($y_{0.5u}$). The interactions between the peripheries of the coherent structures and the uniform parts of the flow are nearly symmetrical in relation to the dynamic mixing layer axis. They reach a maximum value at the mixing

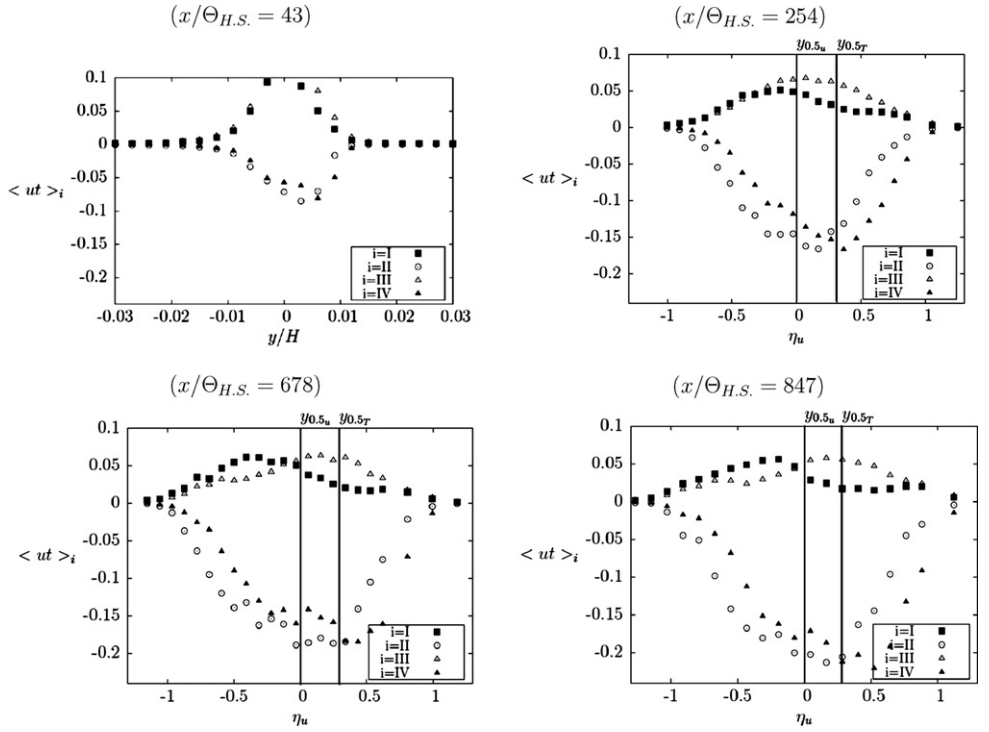

Fig. 10. Transverse profiles of quadrant heat flux contributions, $43 \leqslant x/\Theta_{H.S.} \leqslant 847$ for $r = 0.50$, $\Delta T = 25$ K. $\langle uT \rangle_i$ corresponds to the averaged values of $u'(t) \times T'(t)$ on the ith quadrant.

layer edges, and decrease towards a zero value in the uniform flow region. This corresponds well to the topology of Fig. 8 where quadrants *I* and *III* are held by the cores of the structures in the dynamic mixing zone. In parallel, the magnitude of the contributions of *II* and *IV* becomes greater, reflecting a predominance, within heat flux, of fluid ejections, which behave symmetrically in relation to the thermal mixing region axis (located at $y_{0.5T}$). This growing contribution of quadrants *II* and *IV* corresponds to the shape of the conditional PDFs seen in Section 5.3, where the fluctuations T' associated to the opposite sign of u' are dominant in the self-similarity region.

In the self-similarity region, the dominating movements appear to be ejections. The intensity of the interactions between the periphery of the structures and the outer zones of the uniform flow decreases gradually while the intensity of the ejections increases with *x*. This means that the expansion of the dynamic and thermal mixing layers is associated with a growing domination of saddle point ejections and a weakening interaction between the structures and the outer regions of the mixing layer.

7. Conclusion

The correlations between velocity and temperature fluctuations were investigated across the mixing layer through the ability of the variable temperature hot wire anemometer to deliver simultaneous measurement of velocity and temperature at the same point. The algorithms based on non-linear Levenberg–Marquardt procedures provided access to instant pairs of u and T, with uncertainties around 1% for velocity and 0.15 K for temperature, thus permitting an original analysis of the relationship between velocity and temperature fluctuations at a series of locations across the mixing layer. Conditional PDF analysis emphasized the "marching" behavior of the temperature across the mixing layer in the self-similarity region. Showing a progressive drift from gaussianity as they moved towards the edge, the PDF patterns obtained in the outer and inner regions of the mixing layer could be interpreted in relation to the positivity or negativity associated with the velocity fluctuations. This analysis was performed by means of a quadrant analysis in which the heat flux was split into four components according to the positivity or negativity of $u'(t) \times T'(t)$. This highlighted the growing dominance of the saddle point ejections in the heat flux while moving along the self-similarity region of the mixing layer.

References

[1] H.E. Fiedler, Transport of heat across a plane turbulent mixing layer, Adv. in Geophys. 18A (1974) 93–109.
[2] G.L. Brown, A. Roshko, On density effects and large structure in the turbulent mixing layers, J. Fluid Mech. 64 (1974) 775–816.
[3] R.G. Batt, Turbulent mixing of passive and chemically reacting species in a low speed shear layer, J. Fluid Mech. 82 (1) (1977) 53–95.
[4] S.M. Masutani, C.T. Bowman, The structure of a chemically reacting plane mixing layer, J. Fluid Mech. 172 (1986) 93–126.

[5] D.K. Bisset, Numerical simulation of heat transfer in turbulent mixing layers, in: 13th Australasian Fluid Mechanics Conf., 1998, pp. 21–24.
[6] L.M. Pickett, J.B. Ghandi, Passive scalar measurements in a planar mixing layer by PLIF of acetone, Exp. Fluids 31 (2001) 309–318.
[7] L.M. Pickett, J.B. Ghandi, Passive scalar mixing in a planar shear layer with laminar and turbulent inlet conditions, Phys. Fluids 14 (2002) 985–998.
[8] P.S. Karasso, M.G. Mungal, Scalar mixing and reaction in plane liquid shear layers, J. Fluid Mech. 323 (1996) 23–63.
[9] M. Ndoye, J. Delville, D. Heitz, G. Arroyo, Parameterizable Constant temperature anemometer: a new method for the analysis of velocity–temperature coupling in turbulent heat transfer, Meas. Sci. Technol. 21 (7) (2010) 93–126.
[10] H.H. Bruun, Hot-Wire Anemometry: Principles and Signal Analysis, Oxford University Press Inc., New York, USA, 1995.
[11] A. Perry, Hot-Wire Anemometry, Clarendon Press, Oxford, UK, 1982.
[12] S. Corrsin, Extended applications of hot wire anemometer, Rev. Sci. Ins. 18 (1947) 469–471.
[13] E. Verollet, Contribution aux méthodes de mesure de turbulence, de vitesse et de température par l'anémométrie à fil chaud, Thèse de Doctorat, Université de Marseille, 1965.
[14] L.S.G. Kovasznay, The hot wire anemometer in supersonic flows, J. Aero. Sci. 17 (1950) 565–572.
[15] D.A. Walker, W.F. Ng, M.D. Walker, Experimental comparison of two hot wire techniques in supersonic flow, AIAA J. 27 (1989) 1074–1080.
[16] J. Weiss, H. Knauss, S. Wagner, Experimental determination of the free-stream disturbance filed in a short duration supersonic wind tunnel, Exp. Fluids 35 (2003) 291–302.
[17] M. Saez, Contribution à l'étude expérimentale de la convection mixte, Thèse de Doctorat, Université J. Fourier Grenoble 1, 1998.
[18] M. Ndoye, Anémométrie fil chaud à température variable: application à l'étude d'une couche de mélange anisotherme, Thèse de Doctorat, Université de Poitiers, France, 2008.
[19] W.H. Press, S.A. Teutolsky, W.T. Vetterling, B.P. Flannery, Numerical Recipes in Fortran: The Art of Scientific Computing, second ed., Cambridge University Press, 1992.
[20] BIPM, IEC, IFCC, ILAC, ISO, IUPAC, IUPAP, OIML, Supplement of ISO GUM 95, JCGM 101:2008 – Evaluation of measurement data – Supplement 1 to the Guide to the Expression of Uncertainty Measurement – Propagation of distributions using a Monte Carlo method, 2008.
[21] M.M. Koochesfahani, P.E. Dimotakis, Mixing and chemical reactions in a turbulent liquid mixing layer, J. Fluid Mech. 170 (1986) 83–112.
[22] S.S. Lu, W.W. Willmarth, Measurements of the structure of the Reynolds stress in a turbulent boundary layer, J. Fluid Mech. 60 (1973) 481–511.